Wind and Structures, *Vol. 28, No. 2 (2019) 99-110*
DOI: https://doi.org/10.12989/was.2019.28.2.099

Control effect and mechanism investigation on the horizontal flow-isolating plate for PI shaped bridge decks' VIV stability

Ke Li[*1,2], Guowei Qian[**3], Yaojun Ge[4a], Lin Zhao[4b] and Jin Di[1,2c]

[1]*Key Laboratory of New Technology for Construction of Cities in Mountain Area (Chongqing University), Ministry of Education, Chongqing, China, 400045*
[2]*School of Civil Engineering, Chongqing University, Chongqing, China, 400045*
[3]*Department of Civil Engineering, School of Engineering, The University of Tokyo, 113-8656, Japan*
[4]*State Key Laboratory for Disaster Reduction in Civil Engineering, Tongji University, Shanghai 200092, China*

(Received October 31, 2017, Revised May 28, 2018, Accepted June 5, 2018)

Abstract. Vortex-Induced-Vibration (VIV) is one kind of the wind-induced vibrations, which may occur in the construction and operation period of bridges. This phenomenon can bring negative effects to the traffic safety or can cause bridge fatigue damage and should be eliminated or controlled within safe amplitudes. In the current VIV studies, one available mitigation countermeasure, the horizontal flow-isolating plate, shows satisfactory performance particularly in PI shaped bridge deck type. Details of the wind tunnel test are firstly presented to give an overall description of this appendage and its control effect. Then, the computational-fluid-dynamics (CFD) method is introduced to investigate the control mechanism, using two-dimensional Large-Eddy-Simulation to reproduce the VIV process. The Reynolds number of the cases involved in this paper ranges from 1×10^5 to 3×10^5, using the width of bridge deck as reference length. A field-filter technique and detailed analysis on wall pressure are used to give an intuitive demonstration of the changes brought by the horizontal flow-isolating plate. Results show that this aerodynamic appendage is equally effective in suppressing vertical and torsional VIV, indicating inspiring application prospect in similar PI shaped bridge decks.

Keywords: vortex-induced-vibration; bridge; aerodynamic control; PI shaped deck

1. Introduction

The control of the vortex-induced-vibration (VIV) is a key problem in bridge wind engineering. It commonly takes place in relatively low wind speed, and thus falls into a high probability of occurrence. This phenomenon often starts due to vortex shedding at the deck corners, and then develops into large amplitude oscillations after multiple VIV vibrations occur, where the nonlinear effect of the aerodynamic forces is dominant. It is essential to eliminate or control the VIV of bridge deck, to guarantee the riding comfort and the structural safety.

Since VIV is highly sensitive to the aerodynamic outlines, it is barely possible to find out a universal countermeasure for all types of the bridge decks. However, there is a good chance of several aerodynamic appendages to be valid in a specific deck type. Fig. 1 demonstrates some popular solutions, most of which are only applicable for certain deck types, like the slotted deck or the streamlined box deck. Although a lot of researches have contributed to the investigations of these countermeasures, only some selected studies are included in this paper, for the sake of brevity.

For sections like the parallel arch ribs and the slotted deck (Fumoto *et al*. 2005), it is useful to introduce the barrier. It can prevent the wind from passing through the slotting zone and avoid upper and lower vortices merging into larger ones. This technique was firstly adopted during the construction of the Lupu Bridge, a through arch bridge in China with a central span of 550 m (Ge 2014). The arch ribs are designed to be slotted during operation and covered with the barrier if VIV happens. In following studies, this idea was further developed into solutions of barriers with multi-holes, namely grilles. It is a compromise between the controls of the VIV and the aerodynamic flutter, which could be suppressed if the wind flow can pass through the slotting. Relationships between the grille's opening percentage and its control behavior were studied during the design of the Xihoumen Bridge, a suspension bridge in China with a central span of 1650m (Xiang and Ge 2005).

For streamlined box girders, lots of studies have been carried out to investigate an optimized solution of the faring shape. Most of the studies support a conclusion that sharper faring is beneficial for VIV control (Larsen 2008, Wang 2013, Chen 2016). Except for the faring, guide vane is another useful aerodynamic control appendage. It can be installed at the corners of the bridge deck, accelerating the

∗Corresponding author, Ph.D.
E-mail: keli-bridge@cqu.edu.cn
**Corresponding author, Ph.D.
E-mail: qian@bridge.t.u-tokyo.ac.jp
[a] Ph.D., Professor
E-mail: yaojunge@tongji.edu.cn
[b] Ph.D., Professor
E-mail: zhaolin@tongji.edu.cn
[c] Ph.D., Professor
E-mail: sscsbridge@126.com

ISSN: 1226-6116 (Print), 1598-6225 (Online)

inner wind stream and thus to destroy the downstream vortices (Larsen 1993, Larsenl *et al*. 2000, Sun *et al.* 2012). Alternatively, it can be used as one kind of covers, installed near the inspection rails to make the girder shape streamlined (Nagao *et al.* 1997, Zhang *et al*. 2015). Other trial solutions like installations of the skirt (Fujino and Yoshida 2002) and the separator (Zhang *et al*. 2015), or like adjustments of the crash barriers (Wang *et al.* 2012) and the pedestrian railings (Xia *et al.* 2017) are also attractive, if the VIV problem is severe in streamlined box girder.

As introduced above, these solutions mostly focus on streamlined box girder or bluff girders with inclined web, e.g., cantilevered box girder of the Donghai bridge in China. As for the PI shaped girder, most of the solutions become invalid because of the deck's extremely buff outline. Although adjusting the railing's shapes can suppress the VIV amplitude to some degree, the improved VIV stability still cannot satisfy the safe level required by the local criteria (Qian *et al*. 2015). The PI shaped girder is very popular in cable-stayed bridges due to the attractive economy and convenience in construction and some countermeasures have been tested based on such girder, shown in Fig. 2.

One solution is to re-arrange the two longitudinal girders (Kubo *et al*. 2001). This approach could improve the VIV behavior significantly. But changing the girders' central distance is hard for the designers, who prefer to no substantial modifications of the entire structure. An alternative approach is streamlining with added wind faring (Wardlaw 1972, Qian *et al.* 2015), which has been adopted by the Longs-Creek bridge. However, the introduced extra material and weight will increase the cost remarkably, making further applications limited. Therefore, semi-faring, namely only the upper part of the faring, was proposed (Dong *et al*. 2012) to orient the incoming flow to pass over the railings. Another solution is to suppress the generation of the vortices. As the hollow zone between the pair of the longitudinal girders provides enough space for the vortices to develop and merge into larger ones, lower vertical baffle plates (Macdonald *et al.* 2002, Irwin 2008) or their combination to upper ones(Chen *et al.* 2006) (Zhang *et al.* 2011) were beneficial. The effectiveness of such approach has also been verified during our experiments, but the designers expect some improvement, because overhead welding is not convenient and is hard to guarantee the construction quality. Inspired by this idea, we find out that the horizontal flow-isolating plate shows equal effectiveness in suppressing vertical and torsional VIV.

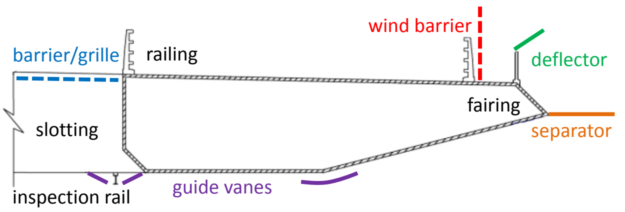

Fig. 1 Aerodynamic countermeasures for VIV control of streamlined box girder

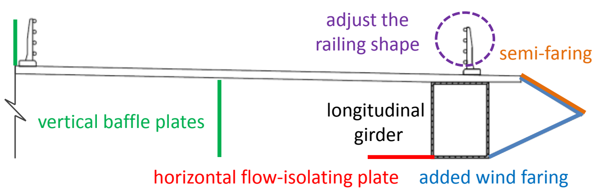

Fig. 2 Aerodynamic countermeasures for VIV control of PI shaped girder

For the above reasons, this paper will introduce the behavior of the horizontal flow-isolating plate. The basic dynamic characteristics and the deck shapes of the involved cable-stayed bridges will be introduced to give the application environment of this technique. The first part of this paper will be about the wind tunnel tests, in which the VIV performance of a bridge sectional model will be tested in cases with and without the horizontal flow-isolating plate. Different plate width and corresponding VIV control results will be examined in different wind attack angles, to check the effectiveness and robustness of this countermeasure. To investigate the control mechanism, CFD method will be introduced in the second part of this paper. The VIV performance will be examined through univariate analysis, making the aerodynamic shape the only changed factor. During the tests, decks with and without the plates will be forced to vibrate in a same specified pattern. An idea of field-filter will be explained in detail, to give an intuitive demonstration of the flow change. Based on this idea, phases and frequencies of the flow field and the surface pressure will be discussed.

2. Wind tunnel tests

A series of wind tunnel tests have been conducted to find out a suitable VIV control countermeasure for a 380 m main-span cable-stayed bridges. The bridge deck uses a pair of boxes as its longitudinal girder, as shown in Fig. 3. Before installing the horizontal flow-isolating plates, several countermeasures have been considered, including reshaping the barriers, changing the inspection rails position, using vertical baffle plates, and installing the semi-faring. Their combinations indeed suppress the VIV amplitudes, but the improved VIV performances still cannot meet the requirements of the standard. Therefore, the horizontal flow-isolating plates were tested, showing inspiring VIV control effects in such PI shaped girders.

2.1 Experimental parameters

The experiments of the VIV control are based on a traditional two-dimensional rigid sectional model of the bridge deck, carried out in the TJ-2 boundary layer wind tunnel in Tongji University, China. The height, width and length of its test section are 2.5 m, 3 m and 15 m, respectively, and the wind speed can be adjusted from 1m/s to 67 m/s, with an interval of 0.1 m/s. Considering the

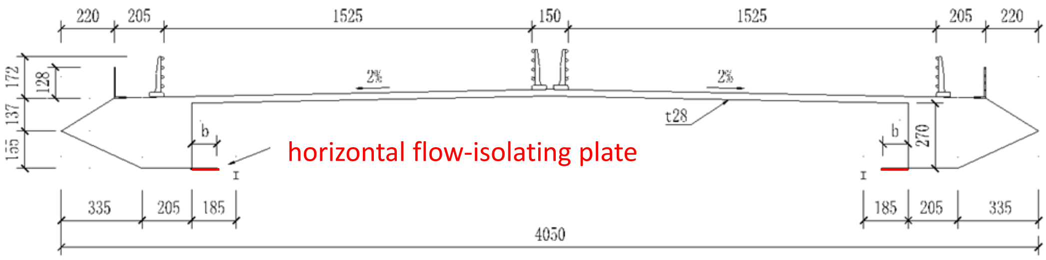

Fig. 3 The bridge girder with the horizontal flow-isolating plate (unit, cm)

Table 1 Properties of the prototype bridge and the down-scaled sectional model

Properties	Unit	Prototype	Similarity ratio	Model
Axial length	m	121.8	1:70	1.74
Equivalent mass	kg/m	46.15×10^3	$1{:}70^2$	9.42
Equivalent mass moment of inertia	$kg \cdot m^2/m$	5806.40×10^3	$1{:}70^4$	0.24
Frequency of heaving mode	Hz	0.41	15.07	6.15
Damping ratio of heaving mode	-	0.33%	-	0.33%
Frequency of pitching mode	Hz	0.79	14.91	11.75
Damping ratio of pitching mode	-	0.17%	-	0.17%


(a) Sectional model of bridge deck


(b) Suspension system

Fig. 4 Two-dimensional sectional model tests in the TJ-2 boundary layer wind tunnel

restriction of the wind tunnel, the down scaling factor of the model's geometry is set to 1:70 to minimize the influence from changed Reynolds number. Affected by some practical factors, the frequency ratios of the heaving and pitching mode are not ideally identical, found to be 15.07:1 and 14.91:1, respectively. The corresponding speed scaling of the vertical VIV and the torsional VIV are therefore 1:4.65 and 1:4.69, respectively. It should be pointed out that these distinctions will not affect the VIV tests, because the VIV phenomenon in bridge engineering barely happens with coupled degrees of the freedom (Sun *et al.* 2013). The major parameters of the prototype bridge and this sectional model are listed in Table 1, in which the equivalent mass m and equivalent mass moment of inertia I are defined in Eq. (1). They represent the participation of the deck's vertical or torsional deformations in a selected mode ϕ. Detials of the equivalent method could be found in the specification (JTG/T 2004) and the book written by Chen (Chen 2005).

The down-scaled model is consisted of a metal framework, some wood surfaces and some plastic-ABS appendages, to guarantee the geometric similarity to the prototype and the rigidity of the shape. The model is anchored to a suspension system shown in Fig. 4. Eight springs and a pair of added counterweights are used to help simulate the frequencies of the selected heaving and pitching modes. Metal strands are twined round the springs to adjust the damping ratio, and wires are used to restrict the deck's shift in the horizontal degree of freedom. During the tests, the deck's motions are monitored by laser sensors, with a sampling frequency of 200 Hz.

(a) Bottom of the bridge girder

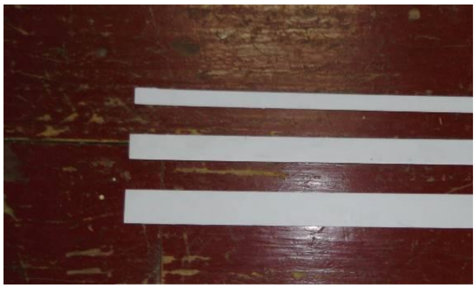

(b) Plates with three different widths

Fig. 5 Sectional model with the horizontal flow-isolating plates

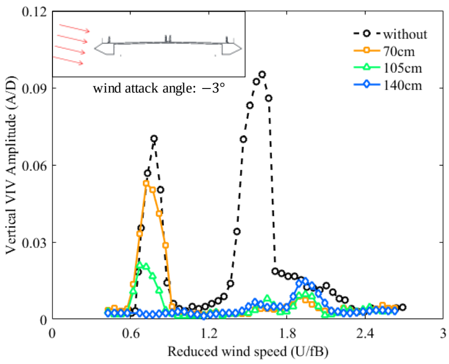

(a) Vertical amplitude under wind attack angle of -3°

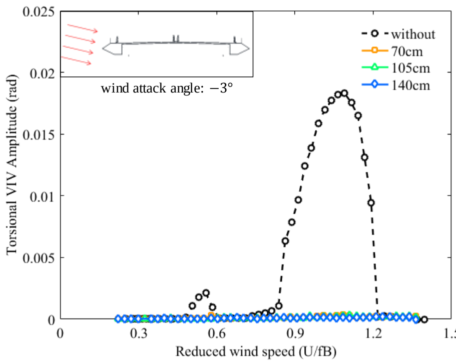

(b) Torsional amplitude under the wind attack angle of -3°

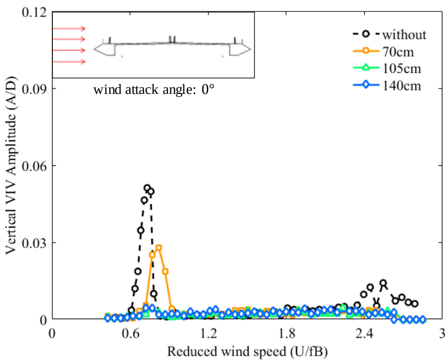

(c) Vertical amplitude under the wind attack angle of 0°

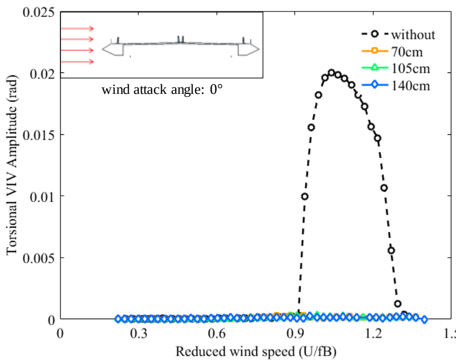

(d) Torsional amplitude under the wind attack angle of 0°

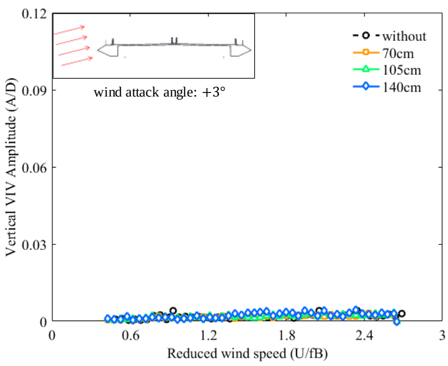

(e) Vertical amplitude under the wind attack angle of +3°

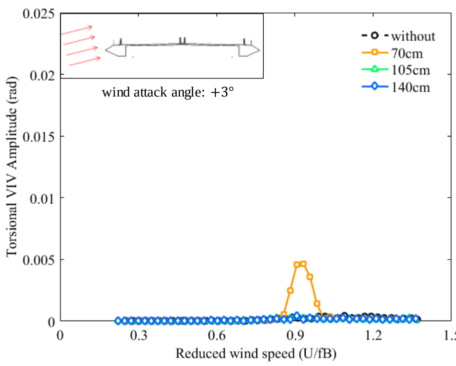

(f) Torsional amplitude under the wind attack angle of +3°

Fig. 6 Deck responses in cases with different horizontal flow-isolating plates

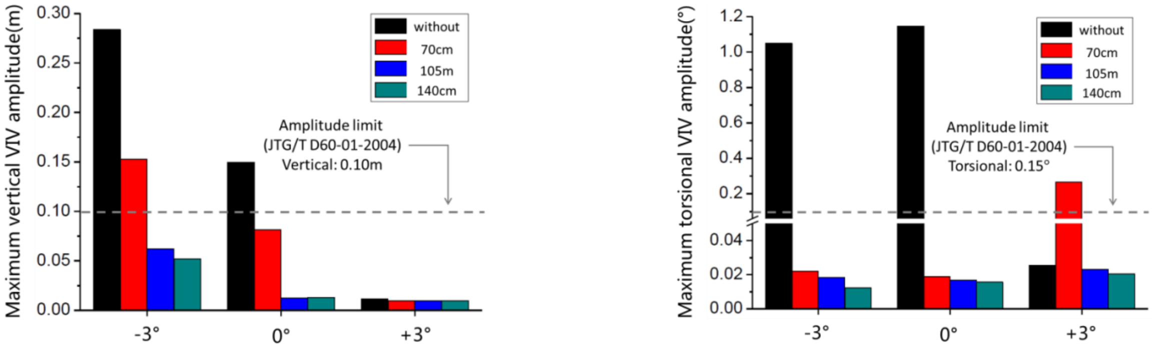

(a) Maximum vertical VIV amplitude (b) Maximum torsional VIV amplitude

Fig. 7 Control results after installation of the horizontal flow-isolating plates

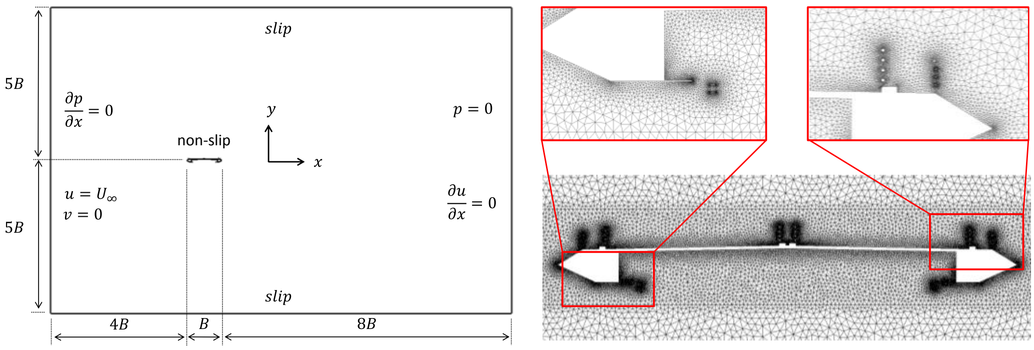

Fig. 8 Details of the two-dimensional computational domain

2.2 VIV performance

To give a conservative conclusion, the wind tunnel tests are carried out in steady incoming flow. Unless specifically explained, all the results mentioned in the following manuscript and figures have been converted to full scale. Cases with three different widths of the horizontal flow-isolating plates are tested in a wide wind speed range, as shown in Fig. 5. Their VIV responses are compared to the original section under three wind attack angles of -3°, 0° and +3°. The plates' widths in a prototype bridge are 70 cm, 105 cm and 140 cm, respectively. Since the mass proportion of the installed plates are 0.45%~0.9%, their influence on the dynamic characteristics are ignored. As shown in Fig. 5, the coordinate dimensions are adjusted to be identical in all cases, to make it convenient to compare the VIV responses. It is noticeable that whatever plate widths were installed, the most unfavorable VIV behavior occurs under the wind attack angle of -3° and 0°. For the original section, significant vertical VIV is observed in two lock-in reduced wind speed regions of 0.5~0.9 and 1.3~1.8, and large torsional VIV appears in the region of 0.8~1.2. The existence of the flow-isolating plates changes little of the lock-in range of the VIV, but significantly reduces the VIV amplitudes in both the vertical degree and the torsional degree. It is noticeable that the 70 cm width plate leads to a new VIV region around reduced wind speeds 0.9, which has been verified by several repeated tests. This phenomenon may result from the strong nonlinear Fluid-Structure-Interaction (FSI) involved in VIV. The possibility of control deterioration when using the horizontal flow-isolating plates should be paid attention to. Except for the torsional VIV with the 70 cm width plate, most cases show a tendency of better VIV suppression effect with wider horizontal flow-isolating plates.

According to the Chinese specification (JTG/T 2004) (JTG/T D60-01-2004), the amplitude limit of the VIV responses in vertical and torsional directions are $[h_a] =$ 0.10m and $[\theta_a] =$ 0.15°, respectively. The citied equations are given by Eq. (2), where f_b and f_t represent bending and torsional frequencies of the prototype bridge, and B denotes the width of the main girder. As shown in Fig. 7, the maximum amplitudes of the vertical and torsional responses are significantly reduced after installation of the horizontal flow-isolating plates. When the plate width is raised to some degree, the VIV response is controlled within the limit.

$$[h_a] = 0.04/f_b \tag{1}$$

$$[\theta_a] = 4.56/Bf_t \tag{2}$$

3. CFD analysis

Though wind tunnel tests have shown the effectiveness of the horizontal flow-isolating plate in bridge VIV control, it is meaningful to further investigate the control mechanism of this countermeasure and to point out its potential ability in similar PI shaped girders. Although the wind tunnel test is commonly used for examining the control behavior, several advantages of the CFD simulation make it more appropriate in mechanism analysis (Morgenthal and Mcrobie 2002). For example, it is convenient to realize forced vibration and to obtain abundant flow field information.

Computer technology has been developed significantly in the past several decades, yet computational cost still remains a significant barrier to wider adoptions of the CFD simulation in bridge engineering, mainly because flows around a bridge deck are highly turbulent, unsteady and three-dimensional. As turbulence is also critical in VIV problem, it is important to reproduce the effect of the vortices to some extent. Therefore, turbulence treatment in the CFD analysis is critical in the coordination between computational cost and accuracy of the solution. The simplest but the most precise treatment is Direct Numerical Simulation (DNS). It does not introduce empirical elements in the calculation, and all scales of the turbulences must be solved using refined meshes and small-time steps. However, bridge VIV occurs at relatively high Reynolds number (about $10^4 \sim 10^5$ in down-scaled sectional models in wind tunnel tests), computational cost for obtaining reliable results becomes unacceptable. Therefore, it is common to introduce empirical model to handle small scale turbulences. RANS approach is an attractive choice which has been widely used in FSI problems. But the time-averaging modeling of turbulence cannot reproduce the response accurately (Miranda *et al*. 2014, Nieto *et al*. 2015), especially when high-frequency aerodynamic forces are dominant.

In this paper, RANS was firstly considered to reproduce the wind tunnel tests, but the results were not satisfying. There were few vortices at the structural frequency, and the calculated VIV amplitude is much smaller. For this reason, Large Eddy Simulation (LES) is adopted as a compromise. It introduces a spatial filter to obtain more precise solution with relatively raw meshes. Behaviors of the LES in two-dimensional computational domain has been checked in simple flow around a cylinder (Sakamoto *et al*. 1993), and its application in bridge engineering has been examined with inspiring results (Bruno and Khris 2003). Considering the prism shape of the bridge girder and the computational cost, it is extremely attractive to investigate the VIV in a two-dimensional domain. In such cases, the span-wise momentum diffusion should be appropriately treated due to the incomplete calculation of the vortices' spatial structure. So, the Smagorinsky constant is adjusted from 0.1 to 0.75 according to prior researches. Due to the above reasons, this paper will introduce LES method to consider the unsteady wind flow in the investigation of the control mechanism.

3.1 Settings of the computational domain

The CFD simulation is carried out using the open-source code OpenFOAM, which is based on a finite volume method. It is developed based on the tensor approach and object-oriented techniques (Weller *et al*. 1998). The PIMPLE scheme is used to uncouple the solution of pressure and flow velocity. It takes advantage of the SIMPLE (Semi-Implicit Method for Pressure Linked Equations) scheme to accelerate convergence and uses the PISO (Pressure Implicit with Splitting of Operators) scheme to obtain transient result at each time step. The schemes for spatial and time discretization are in second order. The spatial schemes for gradient, Laplacian and divergence are Gauss linear, Gauss linear corrected and Gauss limitedLinear, respectively. The implicit backward scheme is used for the time integration. Further details of these schemes can be found in the OpenFOAM 2.2.0.

The overall arrangement is demonstrated in Fig. 8, in which B denotes the width of the deck, and the size of the entire computational domain is 13B by 10B, to reflect the wind tunnel experiments. The coordinate origin locates at the center of the deck. The distances between the boundaries and the deck are large enough to reduce the far field effect, which have been checked in the following FSI verifications. The top and bottom boundaries are 5B away from the center of the deck, and the blockage ratio of the calculation domain is found to be 1.2%.

Dirichlet condition for the flow velocity (u and v) and Neumann condition for the flow pressure p are set as the inlet boundary. Along the outlet boundary, zero normal gradient is specified to the flow velocity , while the pressure is set as zero. The slip condition is applied on the top and bottom boundaries for all variables. No-slip conditions are applied on the surfaces of the deck and the winglet, which means that the flow velocity at the object surface is set to zero when the deck is fixed and is identical to the surface's velocity when the deck is in motion. The internal pressure and velocity fields are set to zero initially and will develop following the boundary conditions. Reynolds number of the cases involved in this paper ranges from 1×10^5 to 3×10^5, with reference length B (width of bridge deck). The eddy viscosity ν_t at the wall is corrected using the Spalding wall function (Spalding, 1961), given as

$$y^+ = U^+ + \frac{1}{E_\kappa}\left(e^{\kappa U^+} - 1 - \kappa U^+ - 0.5(\kappa U^+)^2 - \frac{1}{6}(\kappa U^+)^3\right) \tag{3a}$$

$$y^+ = \frac{\Delta y \cdot U_\tau}{\nu}, \qquad U_\tau = \sqrt{\frac{\tau_w}{\rho}}, \qquad U^+ = \frac{\bar{U}}{U_\tau} \tag{3b}$$

in which $\bar{U}, U_\tau\, \tau_w\, and\, \Delta y$ denote inlet wind velocity, friction velocity, shear stress at wall and distance between the cell center and the wall, respectively. Finally, heights of the near-wall grid are adjusted to set $y^+ < 30$. Instantaneous y^+ at the deck surface is shown in Fig. 9, in which railings are hidden considering expression clarity.

With the horizontal flow-isolating plate installed, the VIV behavior is completely changed, appearing as different aerodynamic shape, different flow, different vibration amplitude, different lock-in wind region, and so on. It is hard to compare two cases in free vibration condition, with so many variables. Therefore, we intend to introduce the principle of single variable. With this idea, the aerodynamic shape is chosen as the only independent variable: with and without the plate; and the flow change will be the dependent variable, which will be studied in forced vibration condition, with identical vibration amplitude and incoming wind speed. To meet this idea, we must choose one wind

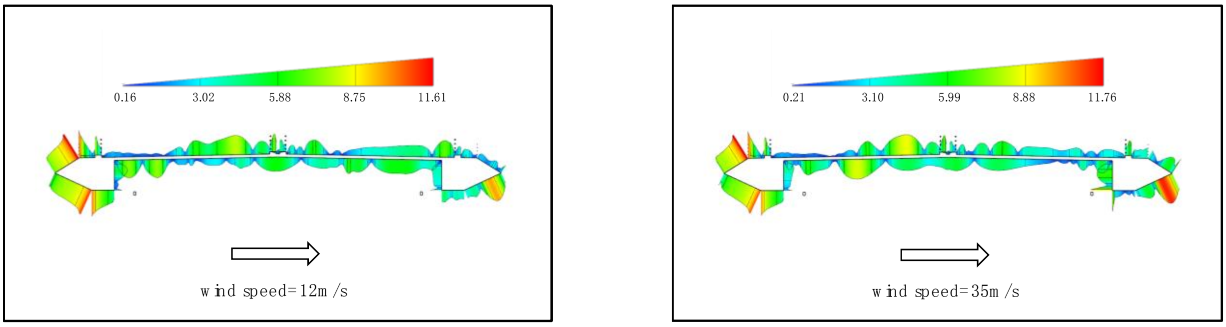

Fig. 9 Instantaneous y^{+} at the deck surface under the tested wind speeds

Table 2 Comparisons of the results between free vibrations in the wind tunnel and the CFD simulation

Target	**Wind speed** (full scale)	**Section types**	**Wind tunnel tests** (full scale)		**CFD simulation** (full scale)	
			frequency	**amplitude**	**frequency**	**amplitude**
Vertical VIV	12 m/s	Original section	0.41 Hz	0.147 m	0.42 Hz	0.112 m
		Section with the plate	0.40 Hz	0.014 m	0.40 Hz	0.035 m
Torsional VIV	35 m/s	Original section	0.79 Hz	0.020rad	0.81 Hz	0.018rad
		Section with the plate	0.79 Hz	0.0003rad	0.78 Hz	0.0008rad

Table 3 Parameter settings of the forced vibration in the CFD simulation

Target	**Wind spee d**	**Frequency**	**Amplitude** (full scale)	**Displacement description**
Vertical VIV	12 m/s	$f_v = 0.41$ Hz	$A_v = 0.112$ m	$D_v(t) = A_v \sin(2\pi f_v t)$
Torsional VIV	35 m/s	$f_t = 0.79$ Hz	$A_t = 0.018$rad	$D_t(t) = A_t \sin(2\pi f_t t)$

speed, where the VIV amplitude is significantly changed after the installation of the horizontal flow-isolating plate.

According to the wind tunnel tests, vertical and torsional VIVs are notably reduced when the wind attack angle is 0°. More importantly, the lock-in wind range with the plate installed is similar to the original section, which will make the following analysis more reasonable. After the installation of the 140 cm plate, the vertical VIV amplitude at wind speed 12 m/s is reduced by 90% and the torsional VIV amplitude at wind speed 35 m/s is reduced by 96%. Based on this fact, FSI simulations are firstly simulated at these two wind speeds, to examine the overall accuracy of the CFD settings. To replicate the process in wind tunnel, the deck is released from zero wind attack angle and zero velocity, and then automatically displaced to the equilibrium position. The involved dynamic parameters are identical to the wind tunnel tests, given in Table 1, and the CFD settings are given in the previous paragraphs. A technique of inverse distance diffusivity (Witteveen and Bijl 2013) is introduced to handle the dynamic mesh. With this method, the overall mesh is treated as an elastic body, and the meshes near the deck undergo small deformations. The key parameters of the simulated results are compared to the ones of the wind tunnel tests, listed in Table 2. It is noticeable that the CFD simulation reproduces the same phenomenon observed in the experiment, that the VIV vibrations are suppressed significantly with the help of the "horizontal flow-isolating plates". The differences between the CFD simulation and the wind tunnel tests are reasonable: it mostly comes from the imperfect reproduction of the flow in the two-dimensional domain. Except that, the VIV phenomenon is indeed reproduced to some extent, laying foundations for the following investigations.

To investigate mechanisms of the passive aerodynamic facilities, CFD method is utilized to give an intuitive comparison of the flow between the cases with and without control. After the installation of the aerodynamic appendage, VIV behavior will change dramatically, resulting from different wind field evolution, different aerodynamic force and different coupling mechanism, etc. To highlight the influence from changed aerodynamic shape, univariate analysis is important. Through driving the optimized deck to vibrate in the same way in which the original deck responses during the VIV, the only changed factor could be kept as the aerodynamic shape. If the applied aerodynamic appendage is beneficial for VIV stability, the aerodynamic effects will show a tendency of doing negative work. The reproduced VIV processes are carried out under two different incoming wind speeds, respectively in the vertical degree and the torsional degree. And the parameters of the forced vibration are given in Table 3.

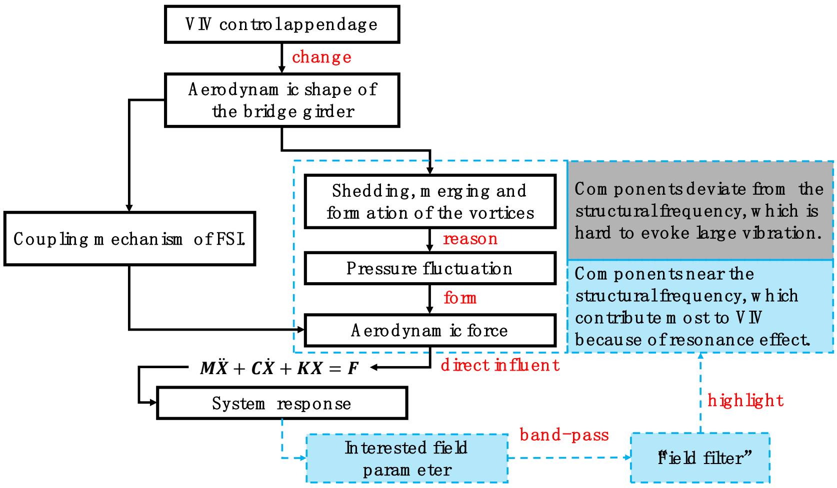

Fig. 10 Ideas of the post-processing based on "field-filter" technique

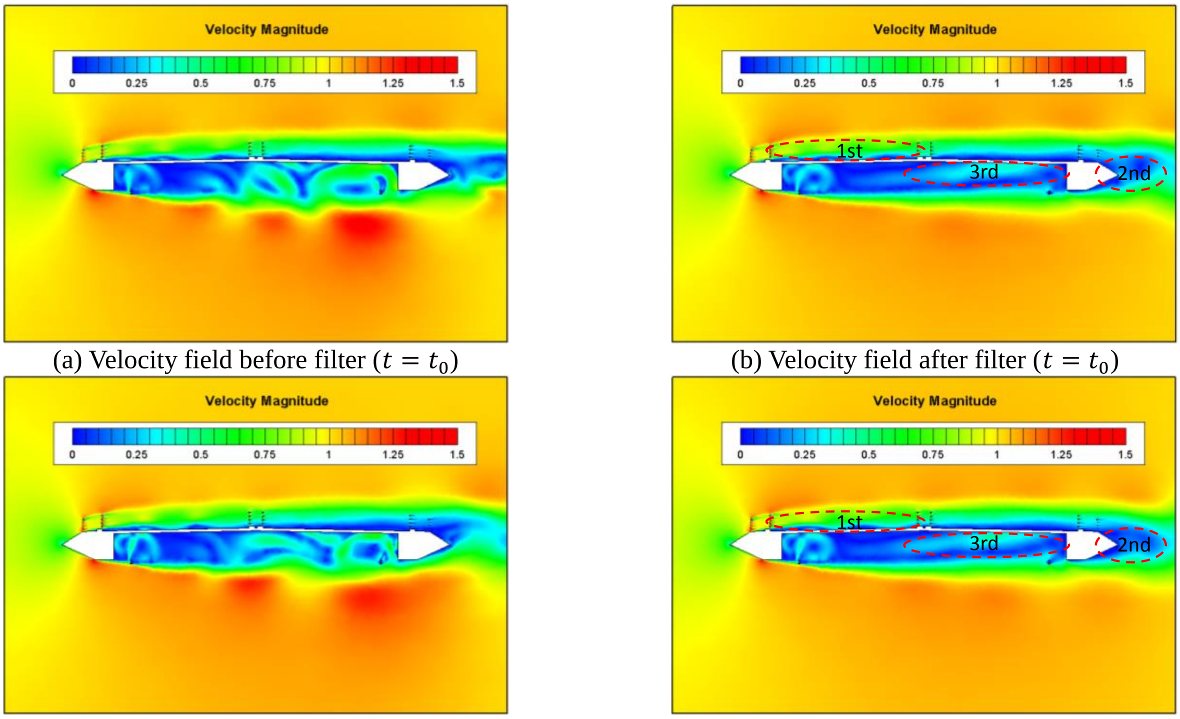

(a) Velocity field before filter ($t = t_0$)

(b) Velocity field after filter ($t = t_0$)

(c) Velocity field before filter ($t = t_0 + 1/f$)

(d) Velocity field after filter ($t = t_0 + 1/f$)

Fig. 11 Vertical VIV reproducing: transient field between original flow and filtered flow (f: VIV frequency)

3.2 Field filter technique

As mentioned before, the VIV phenomenon is highly relative to the vortices in the flow. The complex aero-outline of the bridge deck can produce lots of vortices, shedding from the surfaces of the deck with different frequencies. For PI shaped girders, its aerodynamic shape is far more complex than streamlined girders, making it even more difficult to find out the relationship between the VIV and the numerous vortices. In previous studies, it is common to investigate the control mechanism through observing the changed flow, or the changed surface pressure. From the author's view, some techniques could be introduced to make this process more intuitive. Because only when the frequency of the flow's fluctuation is identical to the natural frequency of the structure, it can induce large amplitude vibration of the VIV (Hua *et al.* 2015). From this reason, it is interesting and meaningful to focus only on the fluctuations with the VIV frequency, which is realized by a post-processing technology based on "field-filter" shown as Fig. 10.

In this method, parameter X denotes what the users care about, which could represent velocity, pressure, amplitude or other fluid parameters. Through introducing a band-pass

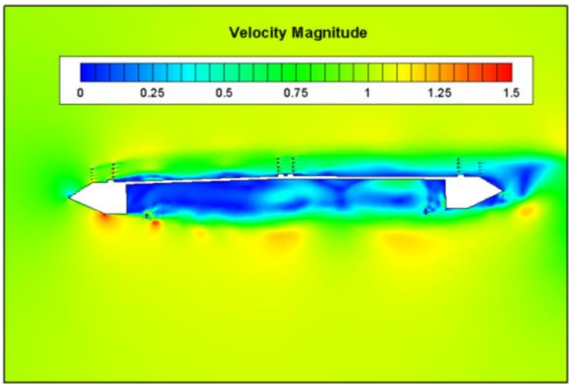

(a) Velocity field before filter ($t = t_0$)

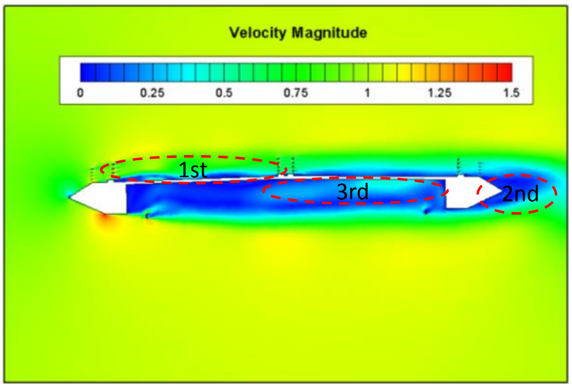

(b) Velocity field after filter ($t = t_0$)

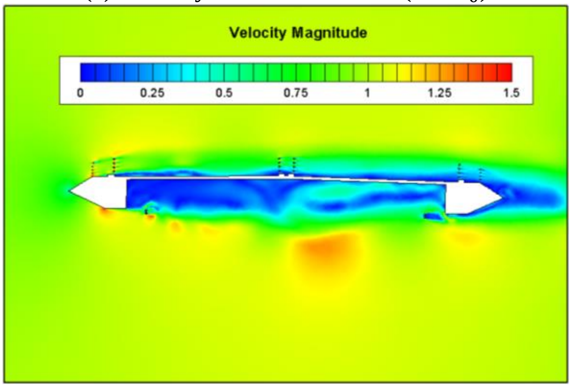

(c) Velocity field before filter ($t = t_0 + 1/f$)

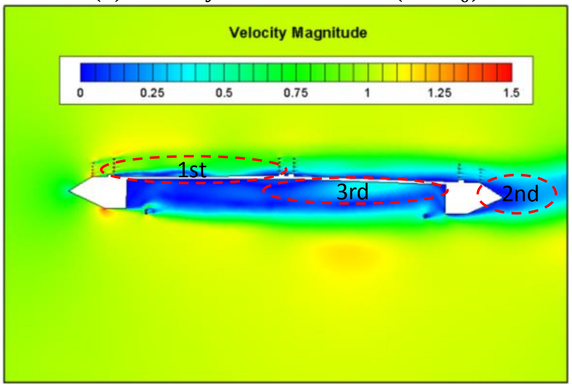

(d) Velocity field after filter ($t = t_0 + 1/f$)

Fig. 12 Torsional VIV reproducing: transient field between original flow and filtered flow (*f*: VIV frequency)

filter, the influence of the concerned parameter X could be emphasized by extracting the fluctuation around a chosen frequency. To be more specified, the time history of the flow field is stored, and the basic variable of the flow at node i can be noted as X_i, which is treated as a superposition of its mean value $\bar{X}_i$ and the fluctuating value x_i. Then, introduce the band-pass filter with a central frequency of the VIV frequency f, noted as $\bigvee_f x_i$. Repeat this process upon each node, and the results of the entire flow field can be expressed as Eq. (4), where $\breve{\boldsymbol{X}}$ emphasizes the fluctuation which affects the VIV most.

$$\breve{\boldsymbol{X}} = \bar{\boldsymbol{X}} + \bigvee_f \boldsymbol{x} \tag{4}$$

When the flow velocity is selected as the filter target, Figs. 11 and 12 respectively demonstrate the vertical and torsional VIV results of the instantaneous velocity magnitude before and after filtering. Two screenshots are given in one time cycle, showing inspiring effects of the field filter technique. It is obvious that the original field data is manifested as a strong unsteady process, and it is impossible to find out the dominant fluctuation relative to the VIV. However, After the filter is applied, researchers could easily identify the most affected zone where potential aerodynamic appendages could be beneficial.

No matter in the vertical case or the torsional case, it could be noticed that the dominant fluctuations mostly locate in three zones: the upper surface between the barriers (1st zone), the leeward zone behind the wind faring (2nd zone), and the lower space between the pair of the longitudinal girders (3rd zone). Researchers have pointed out the optimization of the barrier shape and the installation of the separator could help suppress the VIV (Figs. 1 and 2), which exactly match the first and the second zone. As for the horizontal flow-isolating plate, it just locates in the third zone. This could explain the reason why this countermeasure strongly influent the VIV behavior.

3.3 Control mechanism investigation

As shown in Fig. 10, installed aerodynamic appendages will change the outline of the girder, resulting in different coupling mechanism and vortices forming process. These field factors are the basement of the surface pressure's distribution and fluctuation. Finally, the changed pressure will form the aerodynamic force which directly result in different dynamic response. So, the pressure is the link to connect the VIV response and the changed wind field. It's meaningful to investigate the horizontal flow-isolating plate's influence on the pressure.

To get a deeper view of the control mechanism, fluctuation magnitudes of the filtered pressure field is presented, denoted as $Amp(\breve{C}_p)$ in Eq. (5). It could be regarded as the dominating pressure fluctuation, which represents the most sensitive components that affect the VIV most, based on the resonance theory.

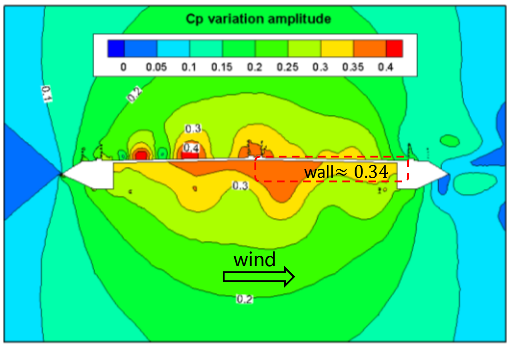

(a) Vertical VIV without the plate

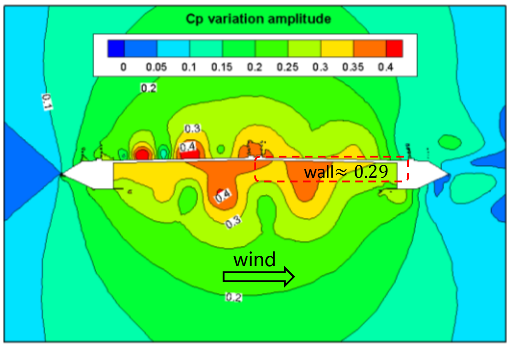

(b) Vertical VIV with the plate

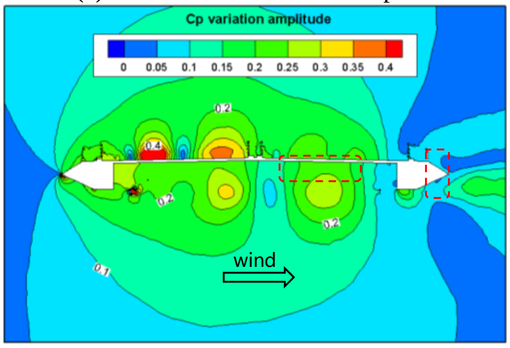

(c) Torsional VIV without the plate

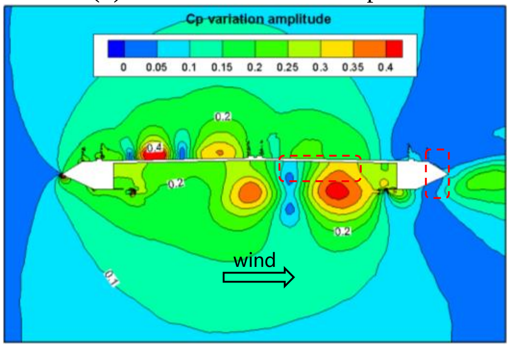

(d) Torsional VIV with the plate

Fig. 13 The dominating pressure fluctuation with and without the horizontal flow-isolating plate

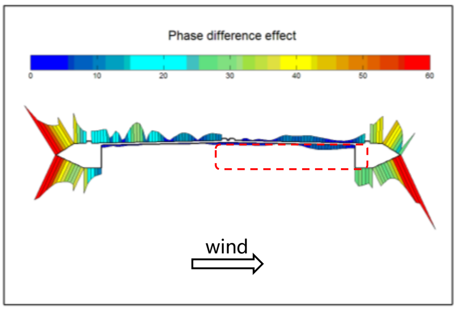

(a) Vertical VIV without the plate

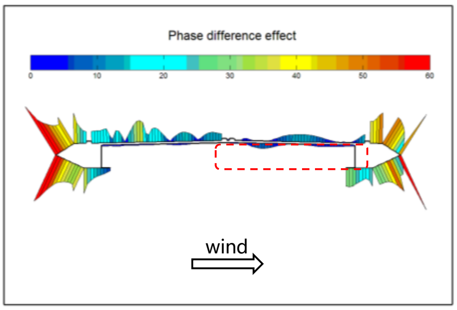

(b) Vertical VIV with the plate

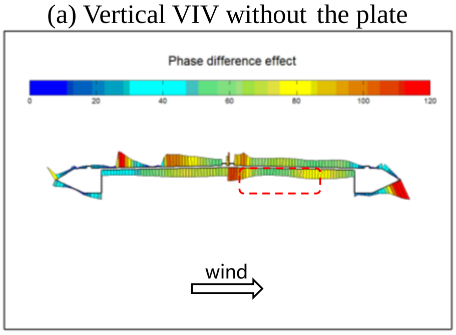

(c) Torsional VIV without the plate

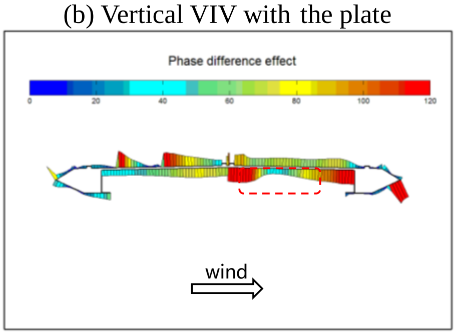

(d) Torsional VIV with the plate

Fig. 14 Changes of the phase difference between the pressure and the aerodynamic force

$$Amp(\breve{\boldsymbol{C}}_p) = \mathcal{F}(\breve{\boldsymbol{C}}_p)\big|_{\omega=2\pi f} \tag{5a}$$

$$\breve{\boldsymbol{C}}_p = \breve{\boldsymbol{P}}(t)/0.5\rho U_\infty^2 \tag{5b}$$

As shown in Figs. 13 and 14, the dominating pressure fluctuations in the lower space and the leeward zone are changed significantly, after the installation of the horizontal flow-isolating plate. For the vertical VIV, mean value of the dominating pressure fluctuation at the lower-leeward surface of the deck is suppressed from 0.34 to 0.29, making the exciting force smaller. As for the torsional VIV, two opposite changes are found at the lower-leeward surface of the deck, making the overall effect complicated. On one hand, vortices in the lower space seem to be amplified after installing the plates. The pressure fluctuation becomes more severe at the lower surface but the distance between the peaks is reduced, resulting ambiguous total toque. On the other hand, the pressure fluctuation at the tail of the deck is suppressed to only half of the original value, changed from 0.1 to 0.05. Since the pressure fluctuation acted on the tail of the deck could effectively form a total torque, the contributions to the diminished torsional VIV may come more from the suppressed vortices shedding behind the deck, than the unfavorable effect brought to the lower space.

As the aerodynamic force is a result of the integrated pressure, the pressure acted on the deck surface can be out of synchronized (Xu *et al.* 2016). Therefore, the phase difference between the pressure and the aerodynamic force is abstracted, to show its contribution to the overall force. If the degree of the phase difference falls into intervals of $[0, 90)$ or $(270, 360]$, the contribution of the pressure is positive to the overall force; and if the degree of the phase difference falls into an interval of $[90, 270]$, the contribution of the pressure is negative to the overall force. In Fig. 14, the phase difference effect is depicted. Higher level means higher relevance between the pressure and the overall aerodynamic force, calculated by the expression of Eq. (6), where $\boldsymbol{R}_{C_p,Force}$ is the cross-correlation function between the force and the pressure; Im and Re means the imaginary part and the real part, respectively.

$$Angle(\boldsymbol{C}_p) = \left| \tan^{-1}\left(Im\left(\mathcal{F}\left(\boldsymbol{R}_{C_p,Force}\right)\right) \middle/ Re\left(\mathcal{F}\left(\boldsymbol{R}_{C_p,Force}\right)\right) \right) \right|_{\omega=2\pi f} \tag{6}$$

From the comparison of Fig. 14 with Fig. 13, the phase difference at the highlighted corresponding zone is noticeable. For both the vertical VIV and the torsional VIV, the relevance between the pressure and the overall aerodynamic force is reduced. This phenomenon should be another explanation for the benefits from the installed horizontal flow-isolating plate.

4. Conclusions

Wind tunnel tests and CFD simulations are carried out to prove the VIV control effect of the horizontal flow-isolating plate. This aerodynamic appendage is supposed to be particularly useful in PI shaped bridge girders. The conclusions are as follows:

- The horizontal flow-isolating plate is proved to be useful in PI shaped girders. Details of the wind tunnel tests of a cable-stayed bridge are presented, showing the VIV behavior is improved in both vertical and torsional degrees.
- Increasing the width of the plate is beneficial in most cases. However, there are chances that some widths may evoke torsional VIV.
- CFD simulation is introduced to reproduce the VIV process of the PI shaped girder, where LES method in two-dimensional computational domain is examined. The results show acceptable accuracy, laying foundations for the following investigations.
- A field-filter technique is used to give an intuitive demonstration of the changes brought by the horizontal flow-isolating plate. Ideas such as dominating pressure fluctuation and phase relevance are explained in detail, to investigate the control mechanism of this appendage.

From the efforts above, potential general control effect of the horizontal flow-isolating plate in similar PI shaped bridge decks can be attractive.

Acknowledgments

The authors gratefully acknowledge the support of National Science Foundation for Young Scientists of China (51808075) 111 Project of China (B18062), China Postdoctoral Science Foundation (2017M620413), Fundamental Reseach Funds for the Central Universities (2018CDXYTM0003) and the Chong-qing Postdoctoral Science special Foundation (XmT2018034)..

References

Bruno, L. and Khris, S. (2003), "The validity of 2D numerical simulations of vortical structures around a bridge deck", *Math. Comput. Model.*, **37**(7), 795-828.

Chen, A., Zhou, Z. and Xiang, H. (2006), "On the mechanism of vertical stabilizer plates for improving aerodynamic stability of bridges", *Wind Struct.*, **9**(1), 59-74.

Chen, Y.Q. (2016), "Aerodynamic shape optimization of central slotted box girders based on performance of wind induced self excited vibration", Master degree, Tongji University.

Chen, Z.Q. (2005), "Bridge wind engineering", China, China Communication Press.

Dong, R., Yang, Y. X. and Ge, Y. J. (2012), "Wind tunnel test for aerodynamic selection of PI shaped deck of cable-stayed bridge", *J. Harbin Inst. Technol.*, **10**, 109-114.

Fujino, Y. and Yoshida, Y. (2002), "Wind-induced vibration and control of Trans-Tokyo Bay Crossing Bridge", *J. Struct. Eng.*, **128**(8), 1012-1025.

Fumoto, K., Hata, K., Matsuda, K. *et al.* (2005), "Aerodynamic improvement of slotted one-box girder section for super long suspension bridge", *Proceeding of the 6th Asia-Pacific Conference on Wind Engineering*, Seoul, Korea.

Ge, Y.J. (2014), "Wind resistance of long span arch bridges", China, China Communications Press Co., Ltd.

Hua, X.G., Chen, Z.Q., Chen, W. *et al*. (2015), "Investigation on the effect of vibration frequency on vortex-induced vibrations by section model tests", *Wind Struct.*, **20**(2), 349-361.

Irwin, P.A. (2008), "Bluff body aerodynamics in wind engineering", *J. Wind Eng. Ind. Aerod*., **96**(6), 701-712.

JTG/T (2004), "Wind-resistent design specification for highway bridges (JTG/T D60-01-2004)", China, China Communication Press.

Kubo, Y., Sadashima, K., Yamaguchi, E., *et al.* (2001), "Improvement of aeroelastic instability of shallow PI section", *J. Wind Eng. Ind. Aerod*., **89**(14-15), 1445-1457.

Larsen, A. (1993), "Aerodynamic aspects of the final design of the 1624 m suspension bridge across the Great Belt", *J. Wind Eng. Ind. Aerod*., **48**(2), 261-285.

Larsen, A. (2008), "Aerodynamic stability and vortex shedding excitation of suspension bridges", *Proceedings of the 4th*

International Conference on Advances in Wind and Structrues (AWAS), Jeju, Korea.
Larsen, A., Esdahl, S., Andersen, J.E., *et al.* (2000), "Storebælt suspension bridge – vortex shedding excitation and mitigation by guide vanes", *J. Wind Eng. Ind. Aerod*., **88**(2), 283-296.
Macdonald, J.H.G., Irwin, P.A. and Fletcher, M.S. (2002), "Vortex-induced vibrations of the Second Severn Crossing cable-stayed bridge - Full-scale and wind tunnel measurements", *Struct. Build*., **152**(2), 123-134.
Morgenthal, G. and Mcrobie, A. (2002), "A comparative study of numerical methods for fluid structure interaction analysis in long-span bridge design", *Wind Struct*., **5**(5), 632-633
Nagao, F., Utsunomiya, H., Yoshioka, E., *et al.* (1997), "Effects of handrails on separated shear flow and vortex-induced oscillation", *J. Wind Eng. Ind. Aerod*., **69**(97), 819-827.
Qian, G.W., Cao, F.C. and Ge, Y.J. (2015), "Vortex-induced vibration performance of a cable-stayed bridge with PI shaped composite deck and its aerodynamic control measures", *J. Vib. Shock*, **34**(2), 176-181.
Sakamoto, S., Murakami, S. and Mochida, A. (1993), "Numerical study on flow past 2D square cylinder by Large Eddy Simulation: Comparison between 2D and 3D computations", *J. Wind Eng. Ind. Aerod*., **50**, 61-68.
Sun, Y., Li, M. and Liao, H. (2013), "Investigation on vortex-induced vibration of a suspension bridge using section and full aeroelastic wind tunnel tests", *Wind Struct*., **17**(6), 565-587.
Sun, Y.G., Liao, H.L. and Li, M.S. (2012), "Mitigation measures of vortex-induced vibration of suspension bridge based on section model test", *J. Southwest Jiaotong Univ*., **47**(2), 219-223.
Wang, D.Z. (2013), "Geometrical optimization of the closed box girders based on aerodynamic performance", Master degree, Tongji University.
Wang, Q., Liao, H.L., Li, M.S., *et al.* (2012), "Influence of aerodynamic shape of streamline box girder on bridge flutter and vortex-induced vibration", *J. Highway Transport. Res. Develop*, **29**(9), 44-50.
Wardlaw, R.L. (1972), "Some approaches for improving the aerodynamic stability of bridge road decks", Canada: National Research Council Press.
Weller, H.G., Tabor, G., Jasak, H., *et al.* (1998), "A tensorial approach to computational continuum mechanics using object-oriented techniques", *Comput. Phys*., **12**(6), 620-631.
Witteveen, J. and Bijl, H. (2013), "Explicit mesh deformation using inverse distance weighting interpolation", *Proceedings of the 9th AIAA Computational Fluid Dynamics.*
Xia, J.L., Li, K., Ge, Y.J., *et al.* (2017), "The crosswind environment and flutter performance of a bridge deck with kinds of wind barriers", *J. Harbin Inst. Technol*., **49**(3), 98-105.
Xiang, H.F. and Ge, Y.J. (2005). "On Areadynamic Limits to Suspension Bridges", *China Civil Eng. J*., **38**(1), 60-68.
Xu, F., Ying, X., Li, Y., et al. (2016), "Experimental explorations of the torsional vortex-induced vibrations of a bridge deck", *J. Bridge Eng*., **21**(12), 04016093.
Zhang, J., Zheng, S.X., Tang, Y., et al. (2015), "Research on optimizing vortex-induced vibration performance for suspension bridge based on section model test", *J. Exp. Fluid Mech*., **29**(2), 48-54.
Zhang, Z.T., Qing, Q.Z. and Xiao, W. (2011), "Vortex-induced vibration and control method for a cable-stayed bridge with open cross section", *J. Hunan Univ.*, **38**(7), 1-5.

AD